ISMEM 2017
- 2nd International Symposium on Multiscale Experimental Mechanics: Multiscale Fatigue

Fatigue damage in non-crimp fabric composites subjected to cyclic bending load

Ulrich A. Mortensen[1]

[1]Section of Composites and Materials Mechanics, Department of Wind Energy, Technical University of Denmark, Frederiksborgvej 399, 4000 Roskilde, Denmark

e-mail: ulmo@dtu.dk

Ulrich Andreas Mortensen, M.Sc. in Mechanical Engineering, Solid Mechanics. PhD-student within the field of fatigue damage and materials processing. Current focus on how micro-scale fatigue damage affects global response composites

1 Introduction

Fatigue life of composites is a very active field of research with predominant focus on tension-tension fatigue. A structural member made from composite material is however likely to be subjected to load cases with significantly different characteristics than those of a tension-tension fatigue test. Bending loads is one load case that have received far less attention compared with tension-tension fatigue. Three point and four point bending tests are the most common test method for testing the static bending properties and standardize methods for employing these tests are available, e.g ASTM D790 [1] and ASTM D7264 [2]. The latter of the two are the main source of inspiration for the bending fatigue test presented in this paper.

Over the past decades a few researchers have reported fatigue testing results based on bending fatigue with four point bending tests [3] [4] [5] and three point bending [6] [7] [8], as well as a few tests based on cantilever beam set-ups [9] [10]. The three and four point tests comes with the advantages of having very simple specimen geometry - most often rectangular cross sections - and generally small nominal forces required by the test machine compared to tension and compression tests. The disadvantages are related to the load introduction where friction becomes an important factor due to the possibility of unwanted

abrasive wear. For thin composite laminates - or generally large span-to-thickness ratio - the geometrically non-linear load-deflection relation arising at large deflection are also a concern that must be adressed. Friction effects are already described in the testing standards for static flexural testing [2] [1] and by Holmberg [11] who included it in a large deflection analysis of four point bending. For the fatigue bending case Paepegem et al. dedicated a whole paper to analysing the influence of friction on the three point bending method [7]. Marsden et al [5] reported issues with abrasive damage when using the 4-point bending method to test fatigue and reported the need to use roller bearings at load and support rollers to diminish friction as well paddings at the contact point between load rollers and specimens to avoid severe abrasive damage.
In this article a four point bending test is used in order to investigate bending fatigue basalt fibre reinforced epoxy material. A geometrically non-linear analysis that includes the effect of friction and support/load roller diameter is introduced and applied to understand the test results. The results are presented in the form of S-N curves and macro-scopic observations of damage in the tested specimens. Finally the results are discussed and the use of optical light microscopy to observe damage at the micro-scale level are discussed for further presentation.

2 Four point bending - Experimental set-up

The four point bending fatigue test were applied on 180 mm long basalt fibre reinforced epoxy specimens with constant rectangular cross sections of 3.6 mm thickness by 20 mm width. The reinforcement of basalt fibres arranged as non-crimp with roughly 90 % of the fibres in the longitudinal direction and roughly 10 % backing bundles in the transverse direction. The longitudinal stiffness of the material was measured to be 32 GPa.

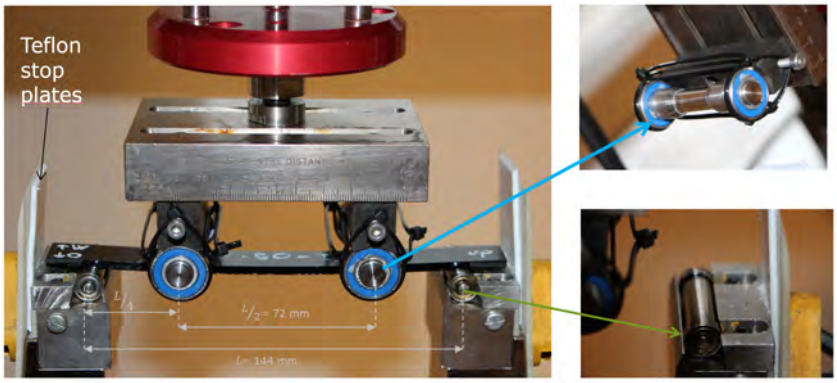

Figure 1: Annotated image highlighting the modifications made to the test-rig in order to achieve good bending fatigue results. Stop plates are made from teflon sheets. The diameter of the load rollers are Ø10 mm where the rollers are in contact with the bending specimens. The support rollers are also of diameter Ø10 mm.

The tests were conducted on an Instron Electropulse E3000 with a ± 5 kN load cell. The machine were fitted with standard four point bending equipment with static load and support rollers of Ø10 mm diameter. The support span (distance between support rollers) was set up to $L = 144$ mm with the load span length $^{L}/_{2} = 72$ mm. The resulting span-to-thickness ratio

is then 40:1, which is 25 % higher[1] than the highest prescribed ratio in the Standards. This ratio was chosen to lower the effects of shear loading and minimize abrasive wear at the point of contact with the rollers. Initial trials of the standard equipment with a loading frequency of 5 Hz showed that it was infeasible to complete any bending fatigue test without modifying the equipment. The main issue preventing tests form being completed was drifting of the specimens in the longitudinal direction of the specimens, which caused them to fall off the testing equipment during testing. The modification to the test method and equipment that has been sustained for the final version of the test are listed in chronological in the list below. The final version of the test equipment is depicted in Figure 1.

1. Stop plates fitted at both ends of the test equipment to prevent specimens from drifting too far of the operational space of the equipment.
2. The static support rollers replaced by Ø10 mm rollers mounted low friction ball bearings.
3. The static load rollers replaced by roller bearing mounted rollers with an inner section of width 20 mm and Ø10 mm diameter and conically rising shoulders.
4. Frequency of loading changed from 5 Hz to 10 Hz

The first modification to the equipment was made out of necessity; no tests could be completed before the drifting issue was resolved. While full tests were completed between making the first and second modifications to the test equipment, the underlying problem of the specimens drifting in the longitudinal direction had not been solved. The specimens kept drifting, and their end points kept scraping against the stop plates causing high level of undesired hysteresis in the load-deflection curves. After the third modification - mounting of bearings on the support rollers - the issue with specimens scraping against the teflon stop plates were reduced to an extent where the tests completed in that configuration were considered acceptable. Thus only tests conducted after the third modification have been included in this paper. The third modification were made to further reduce the effect of friction from rollers and to resolve an issue seen in a few tests where the specimen would rotate around the specimens out-of-plane axis before finally falling of the equipment.The fourth modification further alleviated the issue of the specimens drifting, and in general it seemed to allow the specimens to alternate the direction of drifting (back to forth and back again) until having centered it self with no more drifting.

3 Analysis of the four-point-bending method with large deflection

Testing the beam member specimens with a (support) span-to-thickness ratio of 40:1 is advantageous in terms of limiting effects of shear loading between load and support rollers, as well as limiting abrasive wear at contact points between rollers and beam member specimen. These advantageous does however come at the cost of having large deflection at

[1]The ASTM D7264/D7264M [2] prescribes a span-thickness ratio of 32:1

the load roller positions - and consequently large deflections at the mid-point of the beam member specimen. Large displacements at the load rollers imply that forces in the vertical direction provides contributions to the bending moment in the beam member which must be accounted for. The method that will be applied in this section is based on numerical integration and is similar to a procedure described by Vrooman & Ritter [12], who also analysed the large deflection of the four point bending method, but did not account for the friction between rollers and specimens. The analysis and procedure does not take dynamic effects - velocity and acceleration - into account and assumes that a quasi-static analysis adequately captures the physics of the bending problem at the relatively low loading cycle frequencies[2] applied in the tests. The bending moment in eq. (3) is mathematically identical to a relation given by Holmberg [11] when y is taken at $x = 0$ when $\mu_L = \mu_S$. Equations (3) and (4) are further more identical to Vrooman & Ritter's when the friction is zero ($\mu_L = \mu_S = 0$).

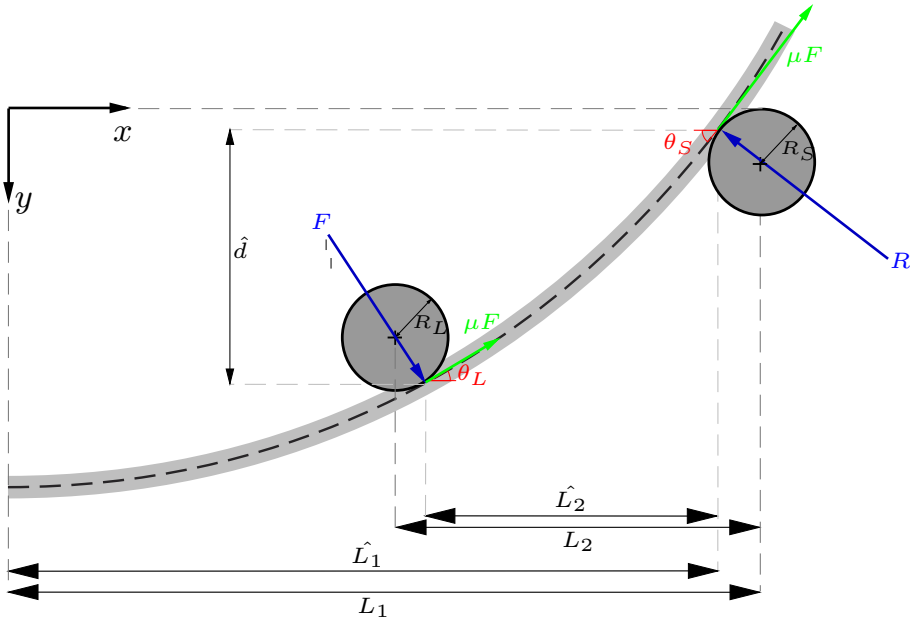

Figure 2: Symmetric half of the beam with imposed forces from the rollers including frictional forces. The schematic employs a coordinate system with $x = 0$ at the beam mid-point (half beam symmetry) and $y = 0$ at the upper vertical tangency point of the support roller.

Figure 2 shows schematically the external forces that contributes to the bending moment in the beam member while in a deformed state. The geometrical thickness of the beam is neglected such that all forces are assumed to work on the beams mid-plane. The coordinate system is chosen with $x = 0$ at the beam mid-point (symmetry-point) and $y = 0$ at the undeformed position of the mid-plane of the beam member. Vertical equilibrium of the beam member provides the relation between the reaction force R at the support roller and the reaction force F at the load roller in eq. (1). A vertical equilibrium for the load roller, which is

[2]The eigenfrequencies of the specimens are over 10 kHz, meaning that they are more than a thousand times higher than the applied frequencies of loading.

externally loaded by[3] $P/2$ and the opposite reaction from F yields eq. (2).

$$R = F\frac{\cos\theta_L - \mu_L \sin\theta_L}{\cos\theta_s + \mu_s \sin\theta_s} \tag{1}$$

$$\frac{P}{2} = \cdot F\left(\cos\theta_L - \mu \sin\theta_L\right) \tag{2}$$

Equations for the bending moments for $0 \leq x \leq \left(\hat{L_1} - \hat{L_2}\right)$ and $\left(\hat{L_1} - \hat{L_2}\right) \leq x\, \hat{L_1}$ can be constructed from the schematic in Figure 2. Applying eqs. (1) and (2) to the moment equilibrium equations allows the formation of eqs. (3) and (4). These equations for the bending moment over the support span provides clear indications that geometrical non-linearities arising from the horizontal components of the reaction forces R and F, and indicates how the non-linearities becomes stronger as the deflection of the beam member specimen becomes larger. Furthermore it should be clear that the friction at the support roller is the more influential than the friction at the load roller due to working on a force with a longer lever.

$$M = \frac{P}{2}\left[\hat{L_1} - x + \underbrace{y\frac{\tan\theta_s - \mu_s}{1 + \mu_s \tan\theta_s}}_{\text{Non-linear term}}\right] \quad \text{for} \quad x \in \left[\hat{L_1} - \hat{L_2}\,;\, \hat{L_1}\right] \tag{3}$$

$$M = \frac{P}{2}\left[\hat{L_2} + \underbrace{y\frac{\tan\theta_s - \mu_s}{1 + \mu_s \tan\theta_s} - \left(y - \hat{d}\right)\frac{\tan\theta_L + \mu_L}{1 - \mu_L \tan\theta_L}}_{\text{Non-linear terms}}\right] \quad \text{for} \quad x \in \left[0\,;\, \hat{L_1} - \hat{L_2}\right] \tag{4}$$

For large angles of θ_S and θ_L the point of contact between the beam member specimen and the rollers are no longer coinciding with the vertical or horizontal center of the rollers, and thus corrections must be made to $\hat{L_1}$, $\hat{L_2}$ and $\hat{d}$. These corrections are given in eqs. (5)-(7).

$$\hat{L_1} = 2a - R_s \sin\theta_s \tag{5}$$

$$\hat{L_2} = a - R_s \sin\theta_s - R_L \sin\theta_L \tag{6}$$

$$\hat{d} = d - R_L\left(1 - \cos\theta_L\right) - R_s\left(1 - \cos\theta_s\right) \tag{7}$$

Equation (8) combined with eqs. (3) and (4) for their respective interevals can be re-casted in to a system of first order differential equations and solved numerically. In this study a fourth order Runga-Kutta[4] scheme was applied. By setting θ_S and P to predefined values, eq. (8) can be integrated first from $x = \hat{L_1}$ to $x = \hat{L_1} - \hat{L_2}$ and then again from $x = \hat{L_1} - \hat{L_2}$ to $x = 0$ with the application of the boundary conditions (eqs. (9)-(11)). This procedure can be iterated with updated guesses for P or θ_S until the condition in eq. (10) is satisfied within a reasonable tolerance. If eqs. (5)-(7) are applied to account for the diameter of the load and

[3] Half of the total force exerted by the machine because of the symmetric half
[4] MatLab's ODE45 solver

support rollers, an initial guess for θ_L must be made and an inner loop of iterations for is required to get the $\hat{L_1}$-length right as well as satisfying $\tan\theta_L = y'$ at $x = \hat{L_1} - \hat{L_2}$.

$$\frac{y''}{\left[1 + (y')^2\right]^{3/2}} = \frac{M}{EI} \tag{8}$$

$$y' = \tan\theta_S \text{ and } y = 0 \quad \text{at} \quad x = \hat{L_1} \tag{9}$$

$$\tan\theta_L = y' \quad \text{at} \quad x = \hat{L_1} - \hat{L_2} \tag{10}$$

$$y' = 0 \quad \text{at} \quad x = 0 \tag{11}$$

The material of the beam members are assumed to behave linear elastically. The maximum stresses in the beam member works at the beam surfaces and are computed using eq. (12), where h is the beam thickness, E the longitudinal stiffness and I the second moment of inertia.

$$\sigma_{max} = \frac{M}{I}\frac{h}{2} \tag{12}$$

4 Results

4.1 Numerical integration scheme

Figure 3 predicts the bending moment along the longitudinal axis of a beam member specimen due to various configurations of friction coefficients at load and support rollers. In Figure 3a the friction coefficient of the load rollers are kept constant at $\mu_L = 0$, while the friction coefficient at the support rollers are varied with $0.0 \leq \mu_S \leq 0.5$. Inspecting Figure 3a reveals that height of ”shoulders” of the bending moment curves are influenced significantly by the friction at the support rollers, while an inspection of Figure 3b - where $\mu_S = 0.0$ and $0.0 \leq \mu_L \leq 0.5$ - shows no such tendency. Both Figure 3a and Figure 3b, with their respective variations of friction coefficients, shows that the inner bending moment - the bending moment in between the load rollers - have a concave shape in the friction-less configuration ($\mu_L = \mu_S = 0.0$). The application of friction at either set of rollers turns the shape of the inner bending moment convex. A concave shape of the inner bending moment is intuitively preferred to a convex shape, as the highest bending moment is positioned away from the contact point with the rollers, thus limiting the risk of having an invalid failure mode due to damage caused by roller contact. Furthermore the friction influence from the loading rollers have a lower impact on the maximum amplitude of the bending moment than friction introduced at the support rollers.
Figure 4 shows a set of different relations between the maximum occuring stress in the beam member specimen and the force or displacement of the beam member at $x = 0$ (midpoint of beam). The relations are generated for various configuration of the friction coefficient. The external force that can be applied to a beam have an upper limit which, when examining Figures 4a and 4b, emphasizes that the force alone is not a good indicator of the level of stress in the specimens. Furthermore the upper limit of the externally applied also

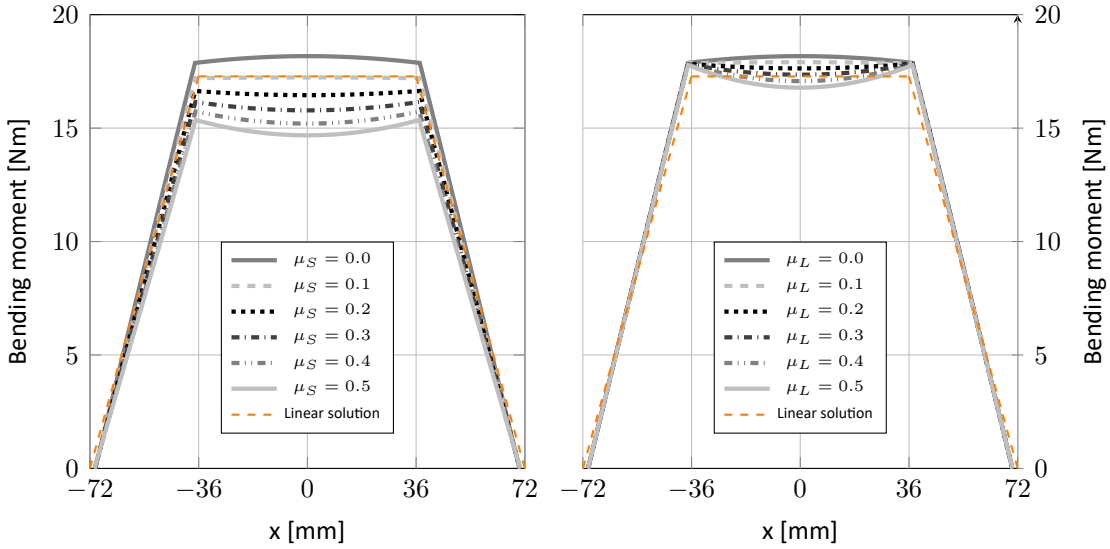

(a) $\mu_S \in [0.0; 0.5]$ and $\mu_L = 0.0$ **(b)** $\mu_L \in [0.0; 0.5]$ and $\mu_S = 0.0$

Figure 3: Change in bending moment over the span of the beam member specimens due to variation in of the friction the load and support rollers respectively when subjected to a total load of $P = 960$ N.

constitutes a practical upper limit to the stress level that can be applied in fatigue testing when the test is run in load control. While Figure 4a may indicate this level is at roughly 1500 N, the test machine used in this study had trouble already in the vicinity of 1200 N, meaning that the stress levels in testing can only reach approximately 500 MPa of max stress. These issues is likely because the load controller have trouble adjusting to the ”softening effect”[5] caused by the geometrical non-linearity.

4.2 Macro-scaled damage

Macro-scale inspection of the tested specimens conclusively reveals that damage occurs where tensional stresses prevail. Figure 5 shows damage on the compression and tension side and the spatial distribution of it related to the bending moment distribution over the longitudinal axis. The pattern of damage on the surface of the specimen showed in Figure 5 is representative of all tested specimens regardless of testing conditions and load levels. The damage shown in Figure 5 also infer very clearly that the damage arises in the part of the specimen situated between the two loading rollers and on the surface of the specimen that is subjected to tensional stresses. On the compression side of the specimen markings are visible due to abrasion from the load rollers, but no significant damage was recorded on any of the specimens as result of the abrasions. A close inspection of the damage on the tension side of the specimen shown in Figure 5 shows that the damage that occurs in the specimens are very likely to be controlled by the pattern of the transverse backing bundles. The markings on the specimen from the loading rollers are minor, and for the support rollers they are not

[5] This is a geometrical effect of the large displacement and does not refer to material softening.

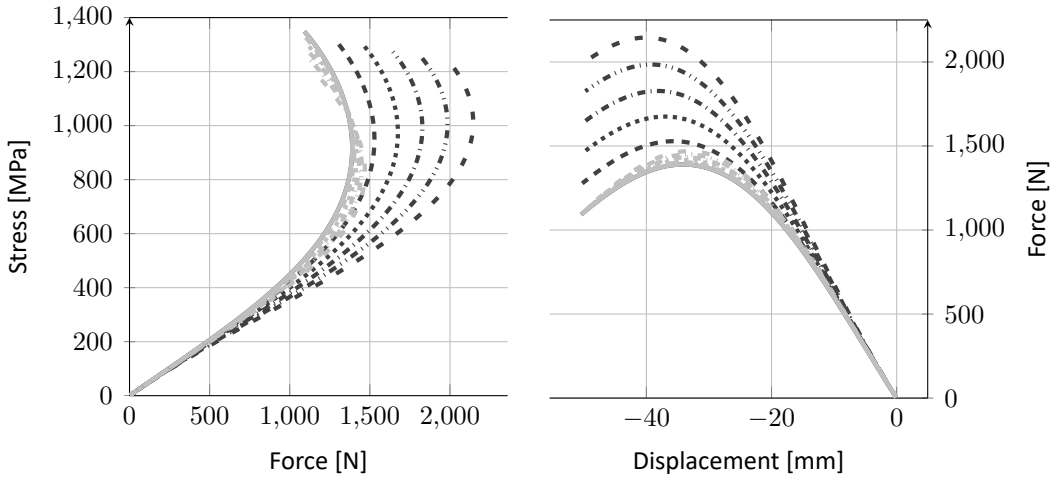

(a) Force - Stress **(b)** Displacement - Stress

Figure 4: Displacement, loading and resulting level of max stresses in the outermost (wrt. to the thickness) material points at the midpoint of the beam ($x = 0$) where symmetry is assumed for varying friction configurations.

distinguishable. These observations should be enough to conclude that the mode of failure for the specimens are due to the imposed bending moment to the specimen and that mode of failure can be described by a consistent damage mechanism that is governed by tensional stresses.

4.3 S-N Curves

Figure 6 shows the S-N curve resulting from all the valid tests performed on the basalt/epoxy material. The points of the S-N curve represent the amount of loading it takes for a specimen to loose 10 % of its flexural modulus for a specific maximum stress level[6]. The stress levels on the second axis of Figure 6 have been computed using the bending moment equations presented in section 3. Trendlines have been added to the S-N plot for two of the represented test conditions. For both conditions the goodness of fit [7] indicates that the test are able to produce consistent results with a level of variance that are most likely attributed to variations in the tested material.

[6]Stress at the outer surface of the specimen at the midpoint of the specimen length.
[7]Represented by the R^2-value

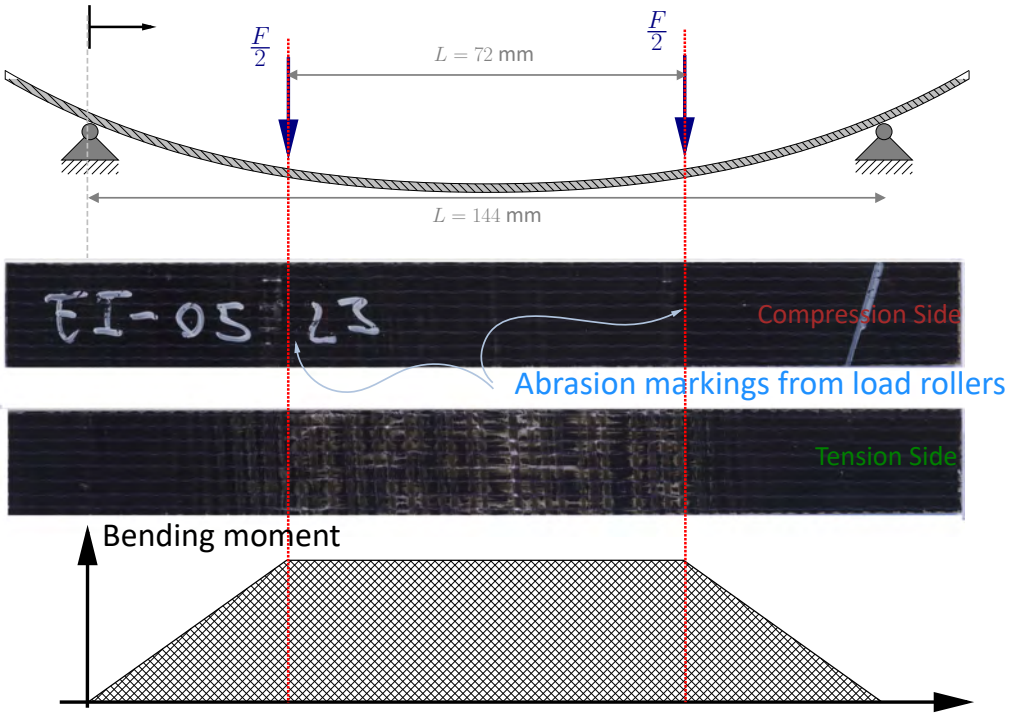

Figure 5: Spatial distribution of macro-scale visible damage on the the specimen related to the moment distribution along the in-plane longitudinal axis of the EI-05-23 specimen.

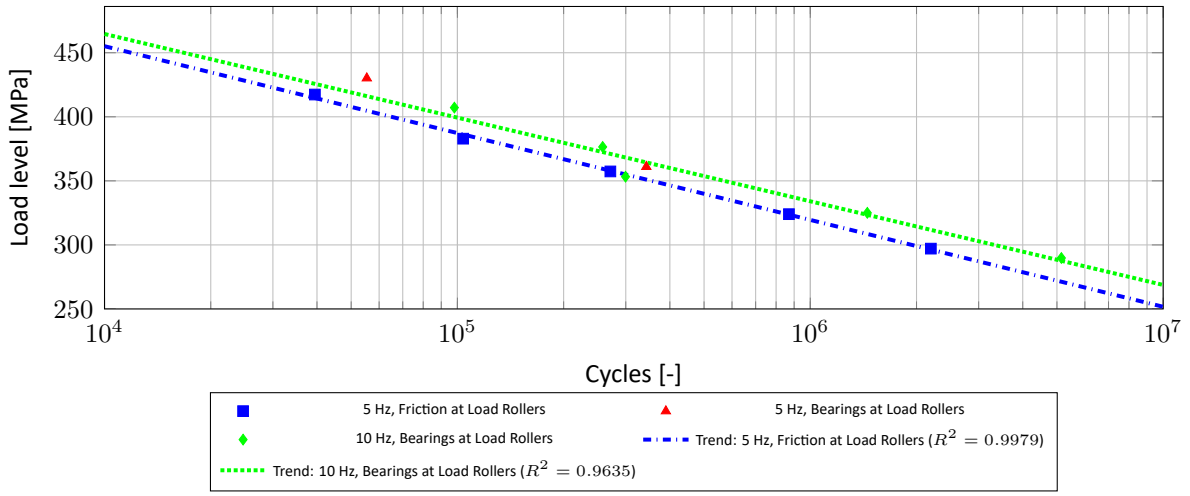

Figure 6: S-N curve for the bending fatigue of the Basalt/Epoxy material tested on the bending equipment. All data points are from tests conducted *after* the mounting of bearings at the *support* rollers.

5 Discussion

The insight of the numerical analysis revealed that friction at the support rollers may play an influential role in the level stress that specimens are subjected to. This is also true for friction at the load rollers, but to a much lesser extent. Decreasing the friction at the load rollers

should theoretically decrease the overall load that the specimens are subjected to, and thus result in higher predicted life time in the S-N curve. The S-N curve shown in Figure 6 do however point in the opposite direction of this conclusion as the specimens tested with reduced friction exhibits better fatigue life properties based on the curve alone. The intuitive explanation to this would be that reducing the friction at the load rollers reduces abrasive damage at the contact points between specimen and load rollers. Inspection of the tested specimens do however renders this explanation unlikely: Little to no damage is found at the load roller contact points of the specimens while extensive amounts of damage exists in the side loaded with tensional stresses well away from any point of contact with load or support rollers. With regards to the variation in the tested material specimens it is worth noting that all the data points represented by the blue squares - and consequently the blue trend-line - were all from the same plate of material and cut adjacent to each other. The consequence of this is that pattern - angle, spacing and cross sectional bundle size - of the transverse backing bundles only vary slightly in this set of specimens. The same statement can be made for all test specimens represented by the green data. The essential meaning of this is that while all specimens tested originate from the same plate of material, the specimens tested before applying bearings to the load rollers - the specimens marked by blue squares - comes from one batch of material, while the specimens tested with a 10 Hz frequency and bearings on the load rollers - the specimens marked by green diamonds - comes from another batch of material. It may thus be reasonable to assume that the difference in fatigue life performance for the configurations with and without friction at the load rollers are caused by differences in the fibre architecture of the two batches of materials rather than the difference in test configurations. This argument is supported by the minuscule amount of abrasive wear found on all specimens tested.
If the above reasoning is accepted this implies that the spacing between the transverse backing bundles constitutes an important property of the specimens and may be imperative to the fatigue life performance of the specimens and consequently the material from which the specimens originate.

6 Conclusion

A set of of relatively simple modifications to a standard method of testing flexural properties have been proposed. The resulting test equipment have been shown to provide consistent test results. A numerical integration scheme have been applied both as means of analysing the influence of frictional forces in the test method as well as to provide accurate measures of stress levels in the test method.
The consistency and relative ease of use of the test method provides a solid stepping stone for using the test method in further research into the damage mechanisms that govern the fatigue life performance of non-crimp fabric composites subjected to cyclic bending loads.
The tested material specimens are clearly affected by the fibre architecture of the non-crimp fabric from which it is produced. The pattern and spacing between the transverse backing bundles constitutes a special area of interest moving forward. The need for a thorough investigation into why the transverse backing bundles in the material, which carries much less load and constitutes a much lower volume fraction of the than the load carrying bundles, have such a high impact on fatigue life is duly noted.

References

[1] "Standard test methods for flexural properties of unreinforced and reinforced plastics and electrical insulating materials," standard, American Society for Testing and Materials.

[2] "Standard test methods for flexural properties of polymer matrix composite materials," standard, American Society for Testing and Materials, West Conshohocken, PA, 2007.

[3] H. Kim and L. Ebert, "Flexural fatigue behaviour of unidirectional fibreglass composites," *Fibre Science and Technology*, vol. 14, pp. 3 – 20, 1981.

[4] G. Shih and L. Ebert, "The effect of the fiber/matrix interface on the flexural fatigue performance of unidirectional fiberglass composites," *Composites Science and Technology*, vol. 28, no. 2, pp. 137 – 161, 1987.

[5] C. Marsden, C. Li, M. Biernacki, and S. J. Carnegie, "4-point bending fatigue testing of thin carbon-epoxy laminates," *Proceedings of the 19th International Conference on COmposite Materials*, 2013.

[6] I. De Baere, W. Van Paepegem, and J. Degrieck, "On the feasibility of a three-point bending setup for the validation of (fatigue) damage models for thin composite laminates," *Polymer Composites*, vol. 29, no. 10, pp. 1067–1076, 2008.

[7] W. V. Paepegem, K. D. Geyter, P. Vanhooymissen, and J. Degrieck, "Effect of friction on the hysteresis loops from three-point bending fatigue tests of fibre-reinforced composites," *Composite Structures*, vol. 72, no. 2, pp. 212 – 217, 2006.

[8] L. Jin, H. Hu, B. Sun, and B. Gu, "Three-point bending fatigue behavior of 3d angle-interlock woven composite," *Journal of Composite Materials*, vol. 46, no. 8, pp. 883–894, 2012.

[9] Y. Tomita, K. Morioka, and M. Iwasa, "Bending fatigue of long carbon fiber-reinforced epoxy composites," *Materials Science and Engineering: A*, vol. 319, pp. 679 – 682, 2001.

[10] W. V. Paepegem and J. Degrieck, "Experimental set-up for and numerical modelling of bending fatigue experiments on plain woven glass/epoxy composites," *Composite Structures*, vol. 51, no. 1, pp. 1 – 8, 2001.

[11] J. A. Holmberg, "On flexural and tensile strength for composites manufactured by rtm," *Journal of Reinforced Plastics and Composites*, vol. 11, no. 11, pp. 1302–1320, 1992.

[12] D. L. Vrooman and J. E. R. Jr, "Nonlinear behaviour of thin beams in four-point bending," *American Ceramic Society Bulletin*, vol. 49, no. 9, pp. 789–793, 1970.